Critical Thrust Force Forecasting for Drilling Exit Delamination of Carbon Fibre Reinforced Plastics

Zhang Lin *, *Hu Jian*, *Tian Wei*, *Liao Wenhe*, *Bu Yin*

College of Mechanical and Electronical Engineering, Nanjing University of Aeronautics and Astronautics, Nanjing 210016, P. R. China

(Received 25 January 2016; revised 5 April 2017; accepted 10 April 2017)

Abstract: Exit delamination is excessive drilling thrust force. Therefore, it is necessary to investigate the critical thrust force which cause exit delamination when carbon fibre reinforced plastics (CRFP) is drilled. According to the linear elastic fracture mechanics, the mechanics of composite material and the classical thin plate bending theory, a common theoretical model of the critical drilling thrust force for CFRP plates is established. Compared with the experimental data of previous studies, the results show that the theoretical values agree well with the experimental values. This model can be used to forecast the critical thrust force for the drilling-induced delamination of CFRP.

Key words: carbon fibre reinforced plastics; standard twist drill; drilling; delamination; critical thrust force

CLC number: V261.97 **Document code**: A **Article ID**: 1005-1120(2017)04-0372-08

0 Introduction

Carbon fibre reinforced plastics (CFRP) features low density, high specific strength and high specific modulus, which are widely used in modern aeronautical manufacturing industry. And compared to metal materials, CFRPs contain unparalleled advantages in the pursuit of high reliability and low weight[1]. CFRP structures need to be connected with screws or rivets after forming. Therefore, the drilling process for the CFRP is inevitable. In automatic assembly process of aircraft parts, hole-making quality is a key factor to ensure riveting quality and the fatigue life of the aircraft structures[2]. However, various hole-making defects have been found in the traditional drilling process. And the delamination defect is viewed as the most significant one which may directly causes aircraft components to be scrapped. Commonly, drilling-induced delamination can be divided into the entry delamination and the exit delamination. It occurs when the interlaminar stress of the CFRP is greater than the adhesive strength of the matrix material at the interfaces during drilling process. The entry delamination is generally less serious; however, the exit delamination is of the main focus of scientific researchers[3].

Research[4] into the formation mechanism of exit delamination in drilling CFRP has shown that as the tool continues to feed during drilling process, the uncut thickness layer of the hole gradually decreases and the bearing capacity of the uncut site gradually weakens. When the uncut site is relatively thin, the thrust force produces a greater deformation, thus causing a Mode I crack failure in the material, from which the exit delamination appears. Many studies[5-7] have found that the size of the delamination defect is closely linked to the magnitude of the drilling thrust force. Reducing the thrust force can reduce the size of the delamination, and exit delamination can be avoided by keeping the thrust force under the critical value. Ho-Cheng et al.[8] analysed the mechanisms that generate push-outdel-

* Corresponding author, E-mail address: zhanglin05@nuaa.edu.cn.

How to cite this article: Zhang Lin, Hu Jian, Tian Wei, et al. Critical thrust force forecasting for drilling exit delamination of carbon fibre reinforced plastics[J]. Trans. Nanjing Univ. Aero. Astro., 2017,34(4):372-379.
http://dx.doi.org/10.16356/j.1005-1120.2017.04.372

amination at exit and peel-up delamination at entrance and firstly forecasted the critical thrust force of drilling-induced exit delamination for composite materials using classical thin plate bending theory and linear elastic fracture mechanics. Feito et al.[9] established two types of finite element models to predict drilling composite delamination defects. The first type is a complete model using the feed rate and the spindle speed as inputs for a complete simulation of the drilling process. While the second type is a simplified model that simulates punching the uncut material with the drilling thrust force as an input. The simulation results of the complete model were verified by experimental data. In addition, the size of the delamination in the simplified model was slightly larger than that in the complete model, indicating that using the simplified model for delamination prediction is more conservative. A study by Rahmé found that the finite element model and the theoretical model with a uniform load predict the drilling-induced delamination of composite materials in terms of critical thrust force relatively consistently. The maximum error in the critical thrust force values predicted by the two types of model was 12%. After the analysis, we can arrive at the conclusion that it is feasible to verify the theoretical model by performing a drill bit punch test on the uncut CFRP material[10].

Qi et al.[11] created a theoretical model of the critical thrust force for the drilling-induced delamination of composite materials that targeted the two laminating states of CFRP/Al and Al/CFRP; the theoretical and experimental results were relatively consistent. Lachaud et al.[12] regarded G_{IC} (the critical energy release rate in mode I) as a variable in relation to the orientation angle between the plies. He established a theoretical model for the critical thrust force under two types of tool/material contact. And the results of the theoretical model with a uniform load were closest to the experimental results. Rahmé et al.[10] considered the effect of the tool's geometric structure on stress state of the uncut material and modelled various hypothetical load states. The experimental results were relatively consistent with the data for a composite load. Due to the anisotropy of composite materials, a model of the critical thrust force for oval-shaped delamination has been established in Ref. [13]. The theoretical results concur with experimental results.

These results show that the primary factors which influence the critical axial force are the material's rigidity, the load's distribution on the thin circular plate, and the processing parameters[14]. To produce delamination-free holes, the drilling methods such as adding backup plate, using various drill types and pre-drilling pilot hole are given in Refs. [15-17], respectively. Based on the study of the critical thrust force, Rahmé et al.[18] investigated the relationship between the thrust force and the process parameters and proposed the critical feed rate. He showed experimentally that when the feed rate was lower than the critical feed rate, the drilling exit delamination did not occur in composite materials. This observation suggested that drilling-induced delamination could be avoided by changing the processing parameters.

A twist drill is the most commonly used tool in drilling CFRP, but the loading conditions of the drill bit's chisel edge and main cutting edge during processing are not exactly the same. This paper assumes that the chisel edge is subjected to a concentrated load and the main cutting edge is subjected to a uniform load, establishes a theoretical model of the critical thrust force for exit delamination of CFRP, and compares the theoretical results with the experimental results reported in Ref. [10]. This model is applicable to twist drills with various geometric parameters and has certain universality. Based on a profound understanding of the critical thrust force for the drilling-induced delamination of composite materials, it has good engineering application value to avoid generating delamination defects by optimizing the tool parameters and improving the tool's force distribution.

1 Prediction of Critical Thrust Force

1.1 Bending stiffness matrix for composite laminated plate

Composite laminated plates are stacked by many single layers with various fibre directions. In the case of plane stress conditions, the stress-strain relationship of composite monolayer in the principle direction is shown as[19]

$$\begin{pmatrix}\boldsymbol{\sigma}_1\\ \boldsymbol{\sigma}_2\\ \boldsymbol{\tau}_{12}\end{pmatrix}=\begin{pmatrix}\boldsymbol{Q}_{11} & \boldsymbol{Q}_{12} & \mathbf{0}\\ \boldsymbol{Q}_{12} & \boldsymbol{Q}_{22} & \mathbf{0}\\ \mathbf{0} & \mathbf{0} & \boldsymbol{Q}_{66}\end{pmatrix}\begin{pmatrix}\boldsymbol{\varepsilon}_1\\ \boldsymbol{\varepsilon}_2\\ \boldsymbol{\gamma}_{12}\end{pmatrix} \tag{1}$$

where $\boldsymbol{\sigma}_{ij}$ and $\boldsymbol{\varepsilon}_{ij}$ are the material's stress and strain components, respectively, in the principle direction. $\boldsymbol{Q}_{ij}$ is the two-dimensional stiffness matrix, which can be expressed in terms of engineering elasticity constants.

$$\boldsymbol{Q}_{11}=\frac{\boldsymbol{E}_{\mathrm{L}}}{1-\boldsymbol{\nu}_{\mathrm{LT}}\cdot\boldsymbol{\nu}_{\mathrm{TL}}},\boldsymbol{Q}_{22}=\frac{\boldsymbol{E}_{\mathrm{T}}}{1-\boldsymbol{\nu}_{\mathrm{LT}}\cdot\boldsymbol{\nu}_{\mathrm{TL}}},$$
$$\boldsymbol{Q}_{12}=\frac{\boldsymbol{\nu}_{\mathrm{TL}}\boldsymbol{E}_{\mathrm{L}}}{1-\boldsymbol{\nu}_{\mathrm{LT}}\cdot\boldsymbol{\nu}_{\mathrm{TL}}}=\frac{\boldsymbol{\nu}_{\mathrm{LT}}\boldsymbol{E}_{\mathrm{T}}}{1-\boldsymbol{\nu}_{\mathrm{LT}}\cdot\boldsymbol{\nu}_{\mathrm{TL}}},\boldsymbol{Q}_{66}=\boldsymbol{G}_{\mathrm{LT}} \tag{2}$$

where $\boldsymbol{E}_{\mathrm{L}}$ is the longitudinal elastic modulus, $\boldsymbol{E}_{\mathrm{T}}$ the transverse elastic modulus, $\boldsymbol{\nu}_{\mathrm{LT}}$ the longitudinal Poisson's ratio, $\boldsymbol{\nu}_{\mathrm{TL}}$ the transverse Poisson's ratio, and $\boldsymbol{G}_{\mathrm{LT}}$ the in-plane shear modulus. For particular composite laminates, the independent engineering elasticity constants are $\boldsymbol{E}_{\mathrm{L}}$, $\boldsymbol{E}_{\mathrm{T}}$, $\boldsymbol{\nu}_{\mathrm{TL}}$ and $\boldsymbol{G}_{\mathrm{LT}}$, $\boldsymbol{\nu}_{\mathrm{LT}}$ can be determined from $\frac{\boldsymbol{\nu}_{\mathrm{L}}}{\boldsymbol{\nu}_{\mathrm{T}}}=\frac{\boldsymbol{E}_{\mathrm{L}}}{\boldsymbol{E}_{\mathrm{T}}}$.

The coordinate system used for presenting a composite layer with a fibre angle of α is shown in Fig. 1. Let $m=\cos\alpha, n=\sin\alpha$. The relationship between stresses in x-y coordinate system and stresses in 1-2 coordinate system is presented as

$$\begin{pmatrix}\boldsymbol{\sigma}_x\\ \boldsymbol{\sigma}_y\\ \boldsymbol{\tau}_{xy}\end{pmatrix}=\begin{pmatrix}m^2 & n^2 & -2mn\\ n^2 & m^2 & 2mn\\ mn & -mn & m^2-n^2\end{pmatrix}\begin{pmatrix}\boldsymbol{\sigma}_1\\ \boldsymbol{\sigma}_2\\ \boldsymbol{\tau}_{12}\end{pmatrix} \tag{3}$$

The relationship between strains in x-y coordinate system and in 1-2 coordinate system is given as

$$\begin{pmatrix}\boldsymbol{\varepsilon}_x\\ \boldsymbol{\varepsilon}_y\\ \boldsymbol{\gamma}_{xy}\end{pmatrix}=\begin{pmatrix}m^2 & n^2 & -mn\\ n^2 & m^2 & mn\\ 2mn & -2mn & m^2-n^2\end{pmatrix}\begin{pmatrix}\boldsymbol{\varepsilon}_1\\ \boldsymbol{\varepsilon}_2\\ \boldsymbol{\gamma}_{12}\end{pmatrix} \tag{4}$$

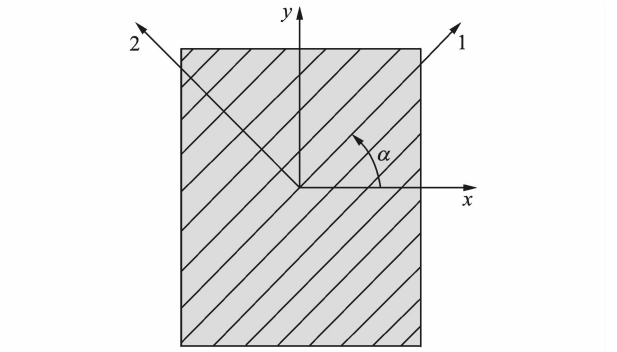

Fig. 1 Laminate with fibre angle α in 1-2 coordinate system and x-y coordinate system

Let $\boldsymbol{T}=\begin{pmatrix}m^2 & n^2 & -mn\\ n^2 & m^2 & mn\\ 2mn & -2mn & m^2-n^2\end{pmatrix}$. The stress-strain relationship of this layer in x-y coordinate system can be obtained by Eqs. (1), (3), and (4)

$$\begin{pmatrix}\boldsymbol{\sigma}_x\\ \boldsymbol{\sigma}_y\\ \boldsymbol{\tau}_{xy}\end{pmatrix}=[\boldsymbol{T}^{-1}][\boldsymbol{Q}][\boldsymbol{T}^{-1}]^{\mathrm{T}}\begin{pmatrix}\boldsymbol{\varepsilon}_x\\ \boldsymbol{\varepsilon}_y\\ \boldsymbol{\gamma}_{xy}\end{pmatrix} \tag{5}$$

Symmetrically laminated plate is a widely used type of composite laminate. And the ply sequence of symmetrically laminated plates and their material properties and geometric sizes are symmetric around a central plane. The coordinate graph of symmetrically laminated plates is shown in Fig. 2. Let $\overline{Q_{ij}}=[\boldsymbol{T}^{-1}]\cdot[\boldsymbol{Q}]\cdot[\boldsymbol{T}^{-1}]^{\mathrm{T}}$. The bending stiffness matrix of symmetrically laminated plates can be written as

$$\boldsymbol{D}_{ij}=\sum_{k=1}^{n}(\overline{\boldsymbol{Q}_{ij}})_k\left(\frac{\boldsymbol{Z}_k^3-\boldsymbol{Z}_{k-1}^3}{3}\right) \tag{6}$$

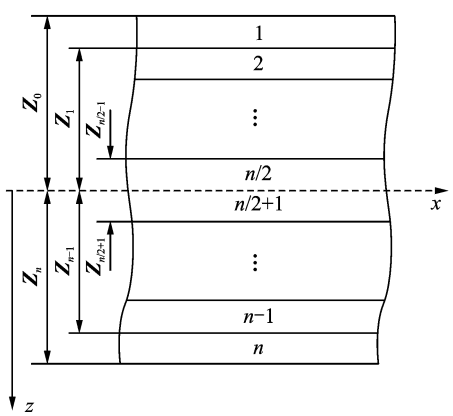

Fig. 2 Coordinate graph of symmetrically laminated plates

1.2 Critical thrust force for drilling-induced delamination of composite materials

Composite laminated plate under thrust force in drilling process produces a plastic bending deformation. When the number of layers remains in the uncut material is little, the plastic deformation area can be regarded as a thin circular plate; the deformation that occurs is bending with small deflection. According to the thin plate bending theory[20], bending with small deflections occur in composite laminates subjected to transverse loads. The differential equation for the elastic surface is given by

$$\boldsymbol{D}_{11}\frac{\partial^4\boldsymbol{\omega}}{\partial x^4}+2(\boldsymbol{D}_{12}+\boldsymbol{D}_{66})\frac{\partial^4\boldsymbol{\omega}}{\partial x^2\partial y^2}+\boldsymbol{D}_{22}\frac{\partial^4\boldsymbol{\omega}}{\partial y^4}=\boldsymbol{q} \tag{7}$$

where ω is the thin plate′s bending deflection and q the undertaking load of the thin plate. The bending deflection of the laminate can be determined by Eq. (7) and the relevant bending boundary conditions.

Based on the virtual work principle, linear elastic fracture mechanics, and the conservation of energy, the work done by the drilling thrust force is equal to the combination of the thin plate′s bending strain energy and the crack propagation energy[8]. Hence, the conservation of energy equation can be expressed as

$$\delta\boldsymbol{W}=\delta\boldsymbol{U}+\delta\boldsymbol{U}\boldsymbol{d} \tag{8}$$

where $\delta\boldsymbol{W}$ is the variation of virtual work done by the thrust force, $\delta\boldsymbol{U}$ the variable quantity of the material′s elastic strain energy, $\delta\boldsymbol{U}\boldsymbol{d}$ the variable quantity of energy in crack growth, which reflects the ability of the material to resist failure due to fracturing.

The strain energy of the bending of a circular thin plate is given by

$$\boldsymbol{U}=\frac{1}{2}\int_s\left[\boldsymbol{D}_{11}\left(\frac{\partial^2\boldsymbol{\omega}}{\partial x^2}\right)^2+2\boldsymbol{D}_{12}\frac{\partial^2\boldsymbol{\omega}}{\partial x^2}\frac{\partial^2\boldsymbol{\omega}}{\partial y^2}+\boldsymbol{D}_{22}\left(\frac{\partial^2\boldsymbol{\omega}}{\partial y^2}\right)^2+4\boldsymbol{D}_{66}\left(\frac{\partial^2\boldsymbol{\omega}}{\partial x\partial y}\right)^2\right]\mathrm{d}s \tag{9}$$

To facilitate subsequent calculations, it is necessary to transform Eq. (9) into a form used in polar coordinate system. Therefore, it is necessary to clarify the transformation between the rectangular and polar coordinate systems (Fig. 3).

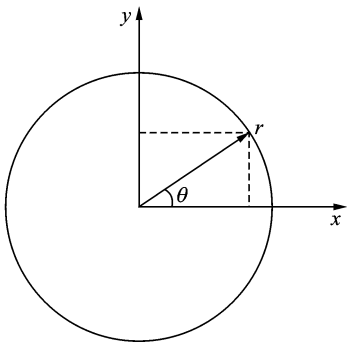

Fig. 3 Transformational relation between rectangular and polar coordinates

From Fig. 3, we can conclude

$$r^2=x^2+y^2,\ x=r\cos\theta,\ y=r\sin\theta \tag{10}$$

The function describing the thin plate′s bending deflection, $\omega=\omega(x,y)=\omega(r,\theta)$, is a continuous function that satisfies the following first order differential equation.

$$\frac{\partial\boldsymbol{\omega}}{\partial x}=\frac{\partial\boldsymbol{\omega}}{\partial r}\frac{\partial r}{\partial x}=\frac{\partial\boldsymbol{\omega}}{\partial r}\frac{x}{\sqrt{x^2+y^2}}$$
$$\frac{\partial\boldsymbol{\omega}}{\partial y}=\frac{\partial\boldsymbol{\omega}}{\partial r}\frac{\partial r}{\partial y}=\frac{\partial\boldsymbol{\omega}}{\partial r}\frac{y}{\sqrt{x^2+y^2}} \tag{11}$$

The second-order differential equation for ω is derived by combining Eqs. (10) and (11).

$$\frac{\partial^2\boldsymbol{\omega}}{\partial x^2}=\frac{\partial^2\boldsymbol{\omega}}{\partial r^2}\cos^2\boldsymbol{\theta}+\frac{\partial\boldsymbol{\omega}}{\partial r}\frac{\sin^2\boldsymbol{\theta}}{r}$$
$$\frac{\partial^2\boldsymbol{\omega}}{\partial y^2}=\frac{\partial^2\boldsymbol{\omega}}{\partial r^2}\sin^2\boldsymbol{\theta}+\frac{\partial\boldsymbol{\omega}}{\partial r}\frac{\cos^2\boldsymbol{\theta}}{r} \tag{12}$$
$$\frac{\partial^2\boldsymbol{\omega}}{\partial x\partial y}=\frac{\partial^2\boldsymbol{\omega}}{\partial r^2}r\sin\boldsymbol{\theta}\cos\boldsymbol{\theta}-\frac{\partial\boldsymbol{\omega}}{\partial r}\frac{\sin\boldsymbol{\theta}\cos\boldsymbol{\theta}}{r}$$

The bending strain energy of circular thin plate can be obtained by Eqs. (9) and (12).

$$\boldsymbol{U}=\frac{\pi}{8}\int_0^a\left[\left(\frac{\partial^2\boldsymbol{\omega}}{\partial r^2}\right)^2(3\boldsymbol{D}_{11}+2\boldsymbol{D}_{12}+3\boldsymbol{D}_{22}+4\boldsymbol{D}_{66})+\frac{\partial^2\boldsymbol{\omega}}{\partial r^2}\left(\frac{1}{r}\frac{\partial\boldsymbol{\omega}}{\partial r}\right)(2\boldsymbol{D}_{11}+12\boldsymbol{D}_{12}+2\boldsymbol{D}_{22}-8\boldsymbol{D}_{66})+\left(\frac{1}{r}\frac{\partial\boldsymbol{\omega}}{\partial r}\right)^2(3\boldsymbol{D}_{11}+2\boldsymbol{D}_{12}+3\boldsymbol{D}_{22}+4\boldsymbol{D}_{66})\right]r\mathrm{d}r \tag{13}$$

The remaining uncut circular thin platedur-ing the drilling process is subjected to a centrosymmetric load, hence, the deflection of the circular thin plate is also centrosymmetric, and

$\int_0^a \frac{\partial^2 \boldsymbol{\omega}}{\partial r^2}\left(\frac{1}{r}\frac{\partial \boldsymbol{\omega}}{\partial r}\right) r\mathrm{d}r = 0$ is obtained through calculations. Let $\boldsymbol{D} = \frac{1}{8}(3\boldsymbol{D}_{11} + 2\boldsymbol{D}_{12} + 3\boldsymbol{D}_{22} + 4\boldsymbol{D}_{66})$, the bending strain energy for circular thin plate is derived by

$$\boldsymbol{U} = \pi \boldsymbol{D}\int_0^a \left[\left(\frac{\partial^2 \boldsymbol{\omega}}{\partial r^2}\right)^2 + \left(\frac{1}{r}\frac{\partial \boldsymbol{\omega}}{\partial r}\right)^2\right] r\mathrm{d}r \quad (14)$$

The primary bearing parts of the twist drill are the chisel edge and the main cutting edge. Usually, the chisel edge bears a concentrated load, and the main cutting edge bears a uniform load. Assuming that the composite thin plate bears the comprehensive effect of the concentrated load $\boldsymbol{F}$, and the uniform load $\boldsymbol{q}$ (Fig. 4), the total thrust force borne by the thin plate is $\boldsymbol{P} = \boldsymbol{F} + \pi \boldsymbol{q} a^2$. Let $\boldsymbol{F}/\boldsymbol{P} = \xi (0 \leqslant \xi \leqslant 1)$, hence, $\pi \boldsymbol{q} a^2 = (1-\xi)\boldsymbol{P}$.

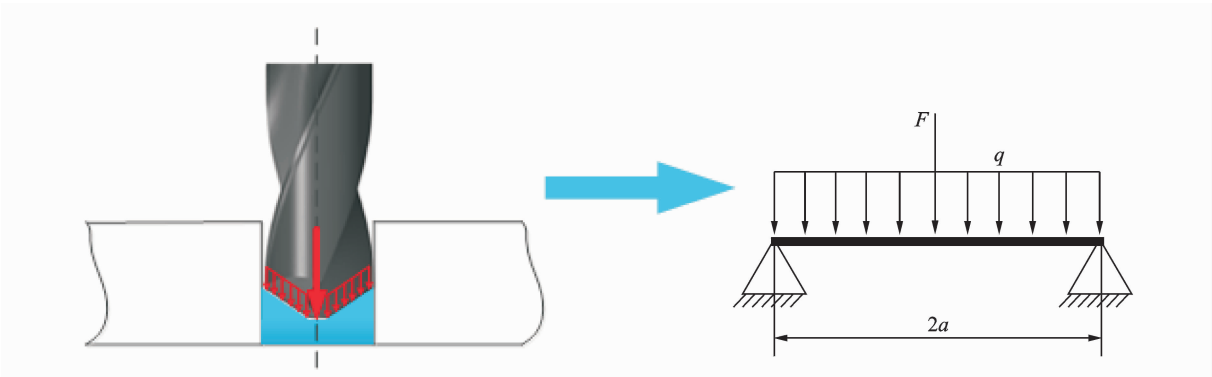

Fig. 4 Load on the composite thin plate

The bending deflection of the thin plate under the effect of the concentrated load F is shown as[20]

$$\boldsymbol{\omega}_1 = \frac{\boldsymbol{F}\left(a^2 - r^2 + 2r^2 \ln\left(\frac{r}{a}\right)\right)}{16\pi \boldsymbol{D}} \quad (15)$$

The bending deflection of the thin plate under the effect of the uniform load q can be obtained[20]

$$\boldsymbol{\omega}_2 = \frac{\boldsymbol{q}(a^2 - r^2)^2}{64\boldsymbol{D}} \quad (16)$$

Based on the superposition principle, the total bending deflection of the thin plate is

$$\boldsymbol{\omega} = \boldsymbol{\omega}_1 + \boldsymbol{\omega}_2 \quad (17)$$

Then, the bending strain energy of the thin plate is given by

$$\boldsymbol{U} = \frac{\pi \boldsymbol{q}^2 a^6}{384\boldsymbol{D}} + \frac{\boldsymbol{F}^2 a^2}{32\pi \boldsymbol{D}} + \frac{\boldsymbol{q}\boldsymbol{F} a^4}{64\boldsymbol{D}} \quad (18)$$

Therefore, the thin plate's variable bending strain energy is

$$\delta \boldsymbol{U} = \left(\frac{\pi \boldsymbol{q}^2 a^5}{64\boldsymbol{D}} + \frac{\boldsymbol{F}^2 a}{16\pi \boldsymbol{D}} + \frac{\boldsymbol{q}\boldsymbol{F} a^3}{16\boldsymbol{D}}\right)\delta a \quad (19)$$

The crack growth energy of the material is

$$\boldsymbol{U}\boldsymbol{d} = \boldsymbol{G}_{\mathrm{IC}} \cdot \boldsymbol{S} = \boldsymbol{G}_{\mathrm{IC}} \pi a^2 \quad (20)$$

where $\boldsymbol{G}_{\mathrm{IC}}$ is the release rate of the Mode I crack growth energy per unit area, $\boldsymbol{S}$ the crack growth area, and a the radius of delamination area.

Then, the variable crack growth energy is

$$\delta \boldsymbol{U}d = 2\boldsymbol{G}_{\mathrm{IC}} \pi a \boldsymbol{\delta} a \quad (21)$$

The work done by the thrust force is calculated by

$$\boldsymbol{W} = \boldsymbol{F} \cdot \boldsymbol{\omega}_{r=0} + \int_0^{2\pi}\int_0^a \boldsymbol{q} \cdot \boldsymbol{\omega}(r) \cdot r\mathrm{d}r\mathrm{d}\theta = \frac{\pi \boldsymbol{q}^2 a^6}{192\boldsymbol{D}} + \frac{\boldsymbol{F}^2 a^2}{16\pi \boldsymbol{D}} + \frac{\boldsymbol{q}\boldsymbol{F} a^4}{32\boldsymbol{D}} \quad (22)$$

$$\delta \boldsymbol{W} = \left(\frac{\pi \boldsymbol{q}^2 a^5}{32\boldsymbol{D}} + \frac{\boldsymbol{F}^2 a}{8\pi \boldsymbol{D}} + \frac{\boldsymbol{q}\boldsymbol{F} a^3}{8\boldsymbol{D}}\right)\delta a \quad (23)$$

Hence, the critical thrust force for delamination defects is determined via Eqs. (11), (19), (21), and (23).

$$\boldsymbol{P}_C = \frac{8}{1+\xi}\pi\sqrt{2\boldsymbol{G}_{\mathrm{IC}}\boldsymbol{D}} \quad (24)$$

2 Numerical Verification and Analysis

This paper proposes using the experimental data in Ref. [10] to verify the theoretical critical thrust force model. The CFRP of T800/M21 with the stacking sequence $[90°, 45°, 0°, -45°]_{10s}$ is used for the experiments, and the thickness of the symmetrically laminated plate is 20 mm. The

fundamental performance parameters of each ply are given in Table 1. A standard tapered sharpened twist drill [DIN1897] without web thinning of diameter 16 mm is used to drill blind hole and punch the uncut material. The experimental set up is shown as Fig. 5. The test was conducted on a CNC machine with a rated power of 25 kW and a maximum speed of 18 000 r/min. Firstly, blind holes were drilled at a cutting speed of 75 m/min and a feed rate of 0.10 mm/r with the uncut layers made of 1 to 6 ply. Then, the motorized spindle punched the uncut material with a constant feed rate and simultaneously an electrically controlled INSTRON traction machine recorded the thrust force. Fig. 6 shows the typical thrust force curve of the uncut material during punching. With the constant extrusion of the drill, the thrust force that acts on the uncut material under the drill increases gradually, as well as the bending deformation of uncut material. When the thrust force reaches the critical value, the first delamination occurs when the thrust force decreases slightly. Then the thrust force increases continuously with the feed of the drill, and the second delamination occurs when the thrust force decreases slightly. The critical value of thrust force that generates first delamination should be defined as the critical thrust force of exit delamination in drilling CFRP.

Fig. 5 Experimental apparatus

Table 1 Fundamental performance parameters of T800/M21

Material	E_L/GPa	E_T/GPa	υ_{LT}	G_{LT}/GPa	G_{IC}/GPa (J·m^{-2})	Ply thickness/mm
T800/M21	160	7.84	0.4	5.22	300	0.25

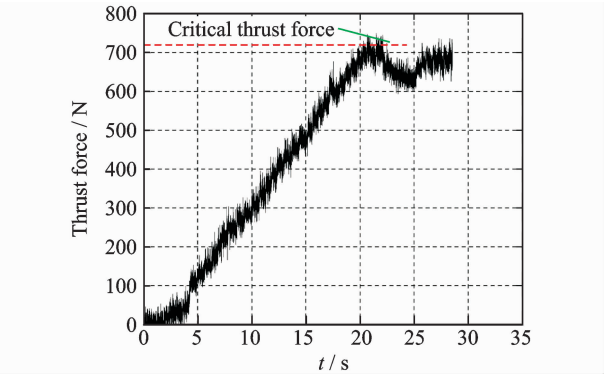

Fig. 6 Thrust force curve during punching

The drilling critical thrust force for exit delamination of T800/M21 is calculated and compared with the experimental data in Ref. [10]. The results are shown in Fig. 7. They demonstrate that the theoretical critical thrust force with a uniform load ($\xi=0$) which neglects the effect of the tool's chisel edge on the uncut material is the highest. While the critical thrust force with a concentrated load ($\xi=1$) that is equivalent to punching the uncut material with flat bottom blind hole by the twist drill's chisel edge is the least. When the number of layers of uncut material is between one and three, the experimental value is slightly higher than the theoretical value, when $\xi=0$. But when the number of layers is more than three, the difference between the two values is greater. While $\xi=0.5$, the theoretical value is less than the experimental value. Generally, the two values are close, which coincides with the situation that the thrust force produced by chisel edge makes up about 50% of total thrust force. And with the increase of uncut layer, the difference between the two values is reduced gradually. The reason for the fluctuations in the theoretical critical thrust force between $8\pi\cdot\sqrt{2\boldsymbol{G}_{IC}\boldsymbol{D}}$ and $4\pi\sqrt{2\boldsymbol{G}_{IC}\boldsymbol{D}}$ is that the different structural parameters of the twist drill changed the distribution of the force on the material. Hence, in order to avoid the delamination defects at the greatest extent, it is available to improve the theoretical critical thrust force by improving the tool's structure and optimizing the tool's load distribution and reduce the drilling thrust force by

optimizing the processing parameters, which needs more investigation in the future.

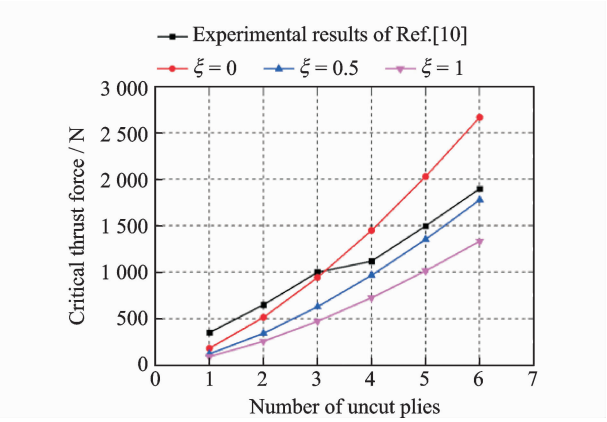

Fig. 7 Comparison between experimental results of Ref. [10] and theoretical values

3 Conclusions

Based on linear elastic fracture mechanics, the mechanics of composite material, and classical thin plate bending theory, the procedure of the establishment of the critical thrust force model is introduced in CFRP drilling with a standard twist drill in detail. This model is general, which takes into account the comprehensive effect of the concentrated load on the chisel edge and the uniform load on the main cutting edge. Moreover, the method to establish the critical thrust force for exit delamination is appropriate for unidirectional laminates and multidirectional laminates.

A comparative analysis of the data obtained from the theoretical model and the experimental results of Ref. [10] shows that the experimental values are in better agreement with the theoretical values when $\xi = 0.5$. In this case, they are also consistent with the actual stress conditions, indicating that this model can be used to predict the critical thrust force for exit delamination and it is conductive to achieving delamination-free hole by properly choosing processing parameters.

Acknowledgments

The authors would like to gratefully acknowledge the financial support of Aeronautical Science Foundations of China (No. 2013ZE52067, No. 2014ZE52057).

References:

[1] GAITONDE V N, KARNIK S R, RUBIO J C, et al. Analysis of parametric influence on delamination in high-speed drilling of carbon fiber reinforced plastic composites[J]. Journal of Materials Processing Technology, 2008, 203(1/2/3):431-438.

[2] TIAN W, ZHOU W, ZHOU W, et al. Auto-normalization algorithm for robotic precision drilling system in aircraft component assembly[J]. Chinese Journal of Aeronautics, 2013, 26(2):495-500.

[3] LIU D F, TANG Y J, CONG W L. A review of mechanical drilling for composite laminates[J]. Composite Structures, 2012, 94(4):1265-1279.

[4] ZHANG H J. Study on the drilling technology of CFRP[D]. Beijing: Beijing University of Aeronautics and Astronautics, 1998: 69-71. (in Chinese)

[5] ZHANG H J, CHEN W Y, CHEN D C. Investigation on delamination defect of hole drilling of CFRP [J]. China Mechanical Engineering, 2003, 14(22): 1978-1980. (in Chinese)

[6] DAVIM J P, REIS P. Study of delamination in drilling carbon fiber reinforced plastics (CFRP) using design experiments[J]. Composite Structures, 2003, 59(4):481-487.

[7] DURÃO L M P, TAVARES J M R S, ALBUQUERQUE V H C D, et al. Damage evaluation of drilled carbon/epoxy laminates based on area assessment methods[J]. Composite Structures, 2013, 96(4):576-583.

[8] HO-CHENG H, DHARAN C K H. Delamination during drilling in composite laminates[J]. Journal of Engineering for Industry, 1990, 112(3):236-239.

[9] FEITO N, LÓPEZ-PUENTE J, SANTIUSTE C, et al. Numerical prediction of delamination in CFRP drilling[J]. Composite Structures, 2014, 108(1): 677-683.

[10] RAHMÉ P, LANDON Y, LACHAUD F, et al. Analytical models of composite material drilling[J]. International Journal of Advanced Manufacturing Technology, 2011, 52(5):609-617.

[11] QI Z, ZHANG K, LI Y, et al. Critical thrust force predicting modeling for delamination-free drilling of metal-FRP stacks[J]. Composite Structures, 2014, 107(1):604-609.

[12] LACHAUD F, PIQUET R, COLLOMBET F, et al. Drilling of composite structures[J]. Composite Structures, 2001, 52(3/4):511-516.

[13] ZHANG L B, WANG L J, LIU X Y. A mechanical model for predicting critical thrust forces in drilling

composite laminates[J]. Proceedings of the Institution of Mechanical Engineers, Part B: Journal of Engineering Manufacture, 2001, 215(2):135-146.

[14] HOCHENG H, TSAO C C. The path towards delamination-free drilling of composite materials[J]. Journal of Materials Processing Technology, 2005, 167(2/3):251-264.

[15] TSAO C C, HOCHENG H. Effects of exit back-up on delamination in drilling composite materials using a saw drill and a core drill[J]. International Journal of Machine Tools & Manufacture, 2005, 45(11): 1261-1270.

[16] HOCHENG H, TSAO C C. Comprehensive analysis of delamination in drilling of composite materials with various drill bits[J]. Journal of Materials Processing Technology, 2003, 140(1/2/3):335-339.

[17] TSAO C C. The effect of pilot hole on delamination when core drill drilling composite materials[J]. International Journal of Machine Tools & Manufacture, 2006, 46(12/13):1653-1661.

[18] RAHMÉ P, LANDON Y, LACHAUD F, et al. Drilling of thick composite material with a small-diameter twist drill[J]. International Journal of Advanced Manufacturing Technology, 2015(76):1543-1553.

[19] SHEN G L, HU G K, LIU B. Mechanics of composite materials[M]. Beijing: Tsinghua University Press, 2013:48-54,164-167. (in Chinese)

[20] TIMOSHENKO S, WOINOWSKY-KRIEGER S. Theory of plates and shells[M]. [S. l.]: McGraw-Hill, 1959: 364-377.

Dr. **Zhang Lin** is currently an assistant professor in Nanjing University of Aeronautics and Astronautics (NUAA). He received his Ph. D. degree from NUAA in 2008. He worked as a visiting scholar in Cranfield University of UK from January, 2015 to January, 2016. His research interests focus on aircraft automated assembly, CNC technology and precision machining technology.

Mr. **Hu Jian** currently works in AVIC Changhe Aircraft Industry (Group) Corporation Ltd. He received his M. S. degree in Manufacturing Engineering of Aerospace from NUAA in 2015. His research interests focus on aircraft automated assembly.

Prof. **Tian Wei** currently works in NUAA. He received his Ph. D. degree in Mechanical Manufacture and Automation from Nanjing University of Scienceand Technology in 2007. His research interests focuse on aircraft intelligent assembly technology.

Prof. **Liao Wenhe** is currently the vice president of Nanjing University of Scienceand Technology. His research interests focus on digital design and manufacturing engineering technology.

Mr. **Bu Yin** is currently a Ph. D. student of NUAA. His recent research interests focus on aircraft intelligent assembly technology.

(Executive Editor: Zhang Tong)